Research Article

Alaulddin A. Al-Jafal* and Suhaib Y. Al-Darzi

Evaluating the interaction for embedded H-steel section in normal concrete under monotonic and repeated loads

https://doi.org/10.1515/eng-2024-0035 received March 05, 2024; accepted April 15, 2024

Abstract: This article presents an experimental investigation into alternative strategies for enhancing the interaction of H-shaped steel sections embedded in normal reinforced concrete. Utilizing 12 push-out specimens subjected to monotonic and repeated loading, the study examines the natural bond-effecting parameters and shear transfer mechanisms facilitated by studs. Key parameters under investigation include embedded length, confinement stirrups, concrete cover, and variations in stud welding configurations, specifically welding to the flange and both the flange and web. In summary, a mathematical model for bond slip was proposed. In enhancing steel-concrete interaction, adding 10mm-diameter studs to both flanges and the web of the steel section is more effective than increasing the embedded depth by 67%. The second most effective method is doubling the concrete cover, followed by increasing the stirrups ratio by 40%. However, adding studs just to flanges outperforms solely increasing the stirrups ratio under repeated loading but does not match the effectiveness of other enhancement parameters. Yet notable shift from brittle to ductile behavior by introducing shear studs attached to flanges. The study also explores the influence of loading type on natural bond, noting lower values (13-18%) in ultimate load and (8-18)% in residual load capacities under repeated loading compared to monotonic loading, this drop is effectively mitigated by shear stud connections, particularly on the flange.

Keywords: bond-behavior, load, slip, shear transfer, studs, push-out test, H-steel section

Suhaib Y. Al-Darzi: Department of Civil Engineering, College of Engineering, University of Mosul, Mosul, Iraq,

e-mail: suhaib.qasim@uomosul.edu.iq

ORCID: Alaulddin A. Al-Jafal 0009-0005-3719-0375; Suhaib Y. Al-Darzi 0000-0002-8437-0193

1 Introduction

Steel reinforced concrete (SRC) is a construction technique where steel sections are integrated into reinforced concrete structures, like columns and walls [1]. The interaction between steel and concrete can improve both the ductility and capacity of the member [2]; the investigation of steel sections embedded in concrete where spanning studies on natural bonding to those on mechanical connections. Previous studies have examined natural bonds, as demonstrated by the studies of Zeng et al. [3], Liu et al. [4], and Bai et al. [5]; on the other hand, the role of mechanical connections has been investigated by Charles Roeder [1], Wang et al. [6], and Hamoda et al. [7], Nevertheless, there is still a deficiency of literature that sufficiently combines the two perspectives and compares natural bonds with enhancement parameters like deeper interaction, confined stirrups, and concrete cover, as well as the advantages of using mechanical connections to support this interaction. Further investigation is needed into alternative strategies to enhance the interaction under monotonous and repetitive loading

Chemical adhesion, friction, and mechanical interlocking are only a few of the factors that contribute to the complex and multifaceted phenomena that are the link between steel and concrete [8]. Chemical adhesion occurs through physical—chemical reactions at the interface of reinforced concrete during the hydration of the cement. This process generates adhesion or capillary forces contributing to the bond between the two materials. After adhesion, the attrition strength is activated, which shows itself when the adhesion is broken. Finally, mechanical interlocking occurs through deformations or ribs on the surface of the steel reinforcement, which increases the surface area available for the concrete to adhere to and induces interlocking effects [9,10].

Numerous researchers have tested the bond behavior of H-shaped steel embedded in different types of concrete under push load. Zeng *et al.* [3] found that the bond stress

^{*} Corresponding author: Alaulddin A. Al-Jafal, Department of Civil Engineering, College of Engineering, University of Mosul, Mosul, Iraq, e-mail: alaulddin.21enp60@student.uomosul.edu.iq

between H-shaped steel and recycled aggregate concrete is inconsistent along the embedded length. The highest stress is at the inner flange interface, the second highest at the outer flange interface, and the web-to-concrete bond stress is comparatively lower. Liu et al. [4] and Bai et al. [5] provided formulas through statistical regression analysis to calculate the average bond stress. These formulas consider multiple factors, including concrete strength, cover thickness, embedded length, lateral stirrup ratio, and recycled coarse aggregate replacement percentage. Liu et al. [11] conducted a push-out test to investigate the bond behavior between shaped steel and high-performance fiber-reinforced concrete: their findings revealed non-uniform steel strain distribution along the embedded length and led to the establishment of an average bond strength-slip constitutive relationship. Huang et al. [12] examined the behavior of H-shaped steel sections embedded in ultrahigh-performance fiber-reinforced concrete (UHPFRC) through experimental and analytical methods. While the bond-slip curves for steel in normal and highstrength concrete were brittle, the curves for steel in UHPFRC displayed ductility and a unique displacement pseudoplastic characteristic. Bai et al. [13] examined the bond behavior of H-shaped steel in engineered cementitious composites, which exhibited superior crack control compared to regular concrete. Bond behavior was outlined by τ -s curves, featuring five stages: non-slip, micro-slip, cracking, descending, and residual.

It's essential to highlight that a mechanical shear connection becomes imperative when the demand for bond stress surpasses the capacity, particularly in scenarios where the section's surface area is relatively small or when a substantial load is necessitated. Charles Roeder [1] conducted tests on two specimens with shear connectors. The findings suggested that shear connectors can introduce local deformations and stress concentrations into the concrete encasement, which, in turn, accelerates the deterioration of the bond due to cracking along the interface. Consequently, it is recommended in the design process to transfer loads by either bond or mechanical methods, avoiding any combination of the two. These observations concerning shear connectors and natural bond stress are unexpected. In contrast, Wang et al. [6] investigated the influence of studs on the bond behavior at the steel-concrete interface. The presence of studs notably enhanced the bond behavior after reaching the peak load, preventing the occurrence of brittle failure observed in naturally bonded specimens. For specimens featuring 13-mm-diameter studs on the flange and web, the residual loads exhibited substantial improvements of 47.1 and 55.0%, respectively, compared to specimens without studs. Furthermore, the relative residual slips increased, underscoring the

advantageous impact of stud placement. Hamoda *et al.* [7] conducted an experimental and numerical investigation on the behavior of steel I-beams with and without high-strength bolted connectors embedded in both normal and steel fiberreinforced concrete (SFRC). In the case of normal concrete specimens, short demountable bolts significantly increased the ultimate load, with more bolts leading to even greater load capacity. A rough I-beam surface also enhanced the ultimate load. Push-out tests showed various failure modes, including minor splitting hairline cracks. To prevent such cracks, closed stirrups were recommended. SFRC specimens exhibited a substantial increase of up to 31% in ultimate load capacity compared to NC counterparts, and steel fibers effectively reduced splitting failures.

1.1 Research significance

The purpose of this study is to experimentally investigate natural bonds and the potential contribution of increasing the main parameters; embedded length, stirrups ratio, and protective cover on the enhancement of natural bonds between the H-steel section and normal concrete alongside the beneficiary of the use of mechanical connections at flange and both flange and web under both the monotonic and repeated load. In addition, establishing a mathematical model for the natural load slip.

2 Experimental programs

2.1 Material and mix proportion

Cement (C) – Portland cement (typ1), IQS:5/2010 [14] – and water (W) – tap water – were used in this investigation. Fine aggregate was the local river sand. Local river rounded gravel as a coarse aggregate IQS:45/2010 [15] was graded with continuous distributions, and their minimum and maximum grain sizes were 10 mm. Table 1 shows that the concrete mix proportions were determined according to ACI211.1-19 [16]. The material properties of the parts used to fabricate the specimens were obtained experimentally. Six cylindrical specimens were fabricated, with dimensions of 150 mm in diameter and 300 mm in height. Three of these specimens were intended to assess concrete compressive strength. At the same time, the remaining three were designated for the evaluation of splitting strength, all following the guidelines outlined in ASTM C39/C496 [17,18]. The results indicated a

Table 1: Mix proportions of concrete (kg/m³)

Cement	Water	Sand	Gravel	Density
400	195	850	890	2,320

mean value of 28 MPa for compressive strength and 2.91 MPa for splitting strength. Table 2 gives the properties of the structural, reinforcement steel, and shear studs. The H-steel section is $200 \times 200 \times 7 \times 10$ mm, and the stud is 50 mm in height.

2.2 Specimens design

Twelve push-out specimens were devised in the experiment to investigate the inherent bonding behavior and shear transfer between steel sections and concrete. Specimen labels encompass a combination of letters and numbers, with "H" denoting steel within concrete. The loading type is signified by "M" for monotonic and "R" for repeated loading, while a two-digit code refines the description: "00" represents control specimens, "01" relates to embedment depth variations, "02" pertains to confinement emphasis, and "03" is for cover thickness. The labels conclude with "S1" or "S2", indicating shear

stud presence on the flange and both the flange and web of the steel section, respectively; 10 mm was the diameter and 50 mm was the length of the shear studs. Table 3 displays the measurements of the push-out specimens. In specimens (HM00, HR00, HM01, and HR01), six strain gauges were placed at 50 mm intervals near the loaded side and 100 mm intervals toward the other side to analyze strain distribution along the flange and web. In other specimens, two strain gauges were located at the mid-depth, one on the flange and one on the web; notably, these intermediate strain gauges were aligned with the vertical positions of the headed studs strategically positioned in between them. This arrangement facilitated an extensive comparison of strain values between the flange and the web.

2.3 Test setup and instrumentation

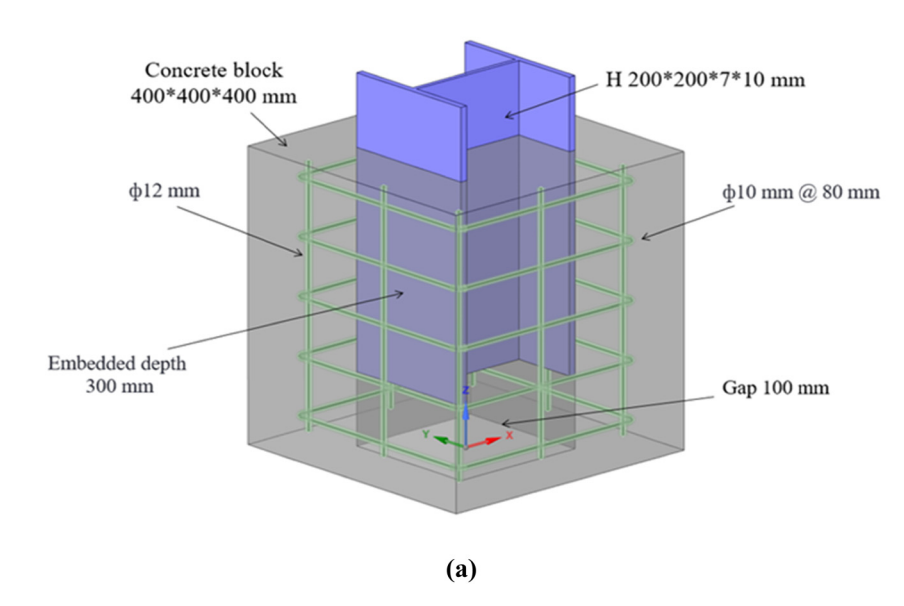
The configuration of the push-out tests and the experimental arrangement, as depicted in Figure 1, for the control specimen, was based on a hydraulic jack system with a 1,000 kN capacity, which was utilized to test the push-out specimens. A steel bearing plate was placed on the section's upper surface to ensure uniform load distribution. To minimize the effects of friction, a layer of fine sand was

Table 2: Steel material properties

Section type	Dimension (mm)	Yield stress f_y (MPa)	ultimate strength $f_{ m u}$ (MPa)	Modulus of elasticity $E_{\rm S}$ (MPa)	Elongation (%)
Steel section (flange)	10	288	412	201	45
Steel section (web)	7	297	422	201	46
Longitudinal bar	Ø12	596	665	200	27
Stirrups	Ø10	450	580	200	30
Shear stud	Shank Ø10 & Head Ø19	429	661	201	34

Table 3: Specimens detail

Specimen	Cover thickness C _s (mm)	Embedded length $L_{\rm e}$ (mm)	Stirrups	Concrete encasement (mm)	Connection type (parameters)	
HM00	100	300	ф10 @ 80 mm	400 × 400	Natural bond	(control)
HR00	100	300	φ10 @ 80 mm	400 × 400		
HM01	100	500	ф10 @ 80 mm	400 × 400	Natural bond	(Embedment)
HR01	100	500	φ10 @ 80 mm	400 × 400		
HM02	100	300	φ12 @ 80 mm	400 × 400	Natural bond	(Confinement)
HR02	100	300	φ12 @ 80 mm	400 × 400		
HM03	200	300	φ10 @ 80 mm	600 × 600	Natural bond	(Cover)
HR03	200	300	φ10 @ 80 mm	600 × 600		
HMS1	100	300	φ10 @ 80 mm	400 × 400	Four studs attached to the flanges	
HRS1	100	300	ф10 @ 80 mm	400 × 400		
HMS2	100	300	ф10 @ 80 mm	400 × 400	Four studs on flanges + Four studs on web	
HRS2	100	300	φ10 @ 80 mm	400 × 400		



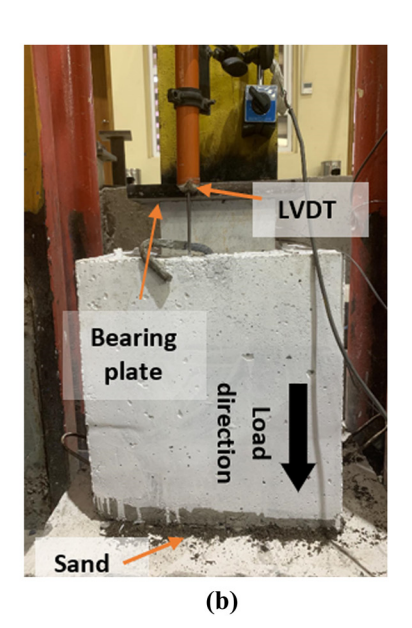


Figure 1: Push-out control specimen: (a) 3D illustration, (b) test set up.

meticulously spread beneath each specimen. Linear variable differential transformers (LVDTs) were meticulously attached to the loaded end of each specimen to precisely measure the displacement of the steel section concerning the concrete encasement. An automated data logger, the TDS-530, was employed for data collection and recording, gathering data from strain gauges (LVDTs) and the load cell. Prior to the initiation of each test, a preloading phase was executed, subjecting each specimen to a load equivalent to 2% of the anticipated ultimate load, making certain that the loading apparatus and the test specimen make appropriate contact. Following this, a monotonic and repeated loading sequence was carried out using a universal testing machine, commencing with an initial loading step at a controlled rate of 15 kN per minute. In the repeated loading test, the initial load was set at 30 kN for the first cycle (10% of the ultimate load for the control specimen). Subsequently, after each cycle, the load was released, and an additional 30 kN was incrementally added for the subsequent cycle (30, 60, 90, 120, 150 kN, and so forth). This loading procedure continued until reaching either the failure load or a slip exceeding 30 mm between the H-steel section and the concrete surrounding it.

3 Experimental results and discussions

3.1 Load slip model of natural bond

The simplified two-part model developed for analyzing the load—slip behavior of structural specimens, such as HM00,

HM01, HM02, and HM03, provides a streamlined yet effective approach to understanding material behavior under load. This model as shown in Figure 2. consists of two distinct phases: a linear ascending phase and an exponential decay phase. The linear ascending phase represents the initial proportional increase in load with increasing slip, capturing the elastic or linear behavior of the material up to its ultimate load-bearing capacity. This phase is characterized by a constant slope, calculated as the ratio of the ultimate load to the corresponding slip at that load, effectively modeling the initial stiffness and strength of the material.

Once the ultimate load is reached, the model transitions into the exponential decay phase. This second phase

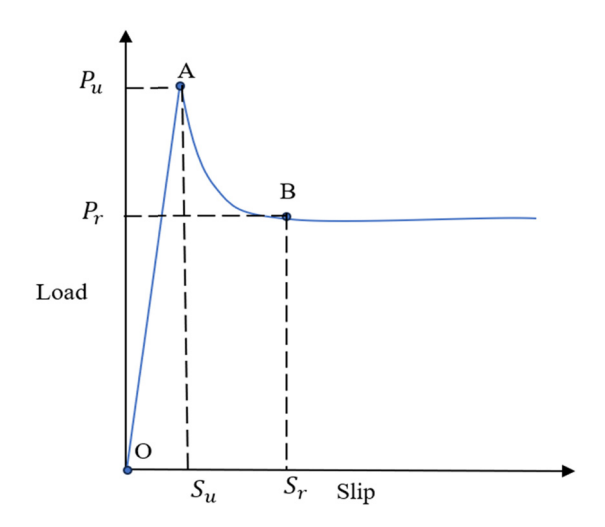


Figure 2: Load-slip curve for natural bond.

illustrates the material's behavior beyond its peak load, often associated with the onset of damage, yielding, or other non-linear behaviors. The exponential decay is governed by a decay constant, which determines the rate at which the load decreases with increasing slip. This part of the model adeptly simulates the gradual reduction in loadbearing capacity, providing insights into the post-peak response of the material. Notably, the model's parameters, including the ultimate load, slip at ultimate load, and decay constant, can be adjusted to fit different specimens, making it a versatile tool for analyzing a range of load-slip behaviors. The model's simplicity, combined with its ability to adapt to different specimens, makes it a valuable resource for predicting and understanding structural performance under various loading conditions. The equation representing the simplified two-part model for analyzing the load-slip behavior of structural specimens is as follows:

$$P_{(\mathrm{Slip})} = \begin{cases} k \times \mathrm{slip} & \mathrm{Slip} \leq S_{\mathrm{u}} \\ P_{\mathrm{r}} + (P_{\mathrm{u}} - P_{\mathrm{r}})e^{-\beta(\mathrm{Slip} - S_{\mathrm{u}})} & \mathrm{Slip} \geq S_{\mathrm{u}} \end{cases},$$

where $P_{\text{(Slip)}}$ is the load in kN as a function of the slip in mm, $k = \frac{P_{\text{u}}}{S_{\text{u}}}$ is the slope of the linear ascending phase, determined by the ultimate load and slip, P_{u} is the ultimate load for the specimen in kN, S_{u} is the slip at ultimate load in mm, β is the decay constant 0.28, and P_{r} is the residual load, calculated as a percentage of the ultimate load (70% P_{u}).

3.2 Ductility assessment

Eurocode 4 designates the slip capacity (δu) as the crucial measure for assessing the ductility of shear connectors. Representing the slip value where the characteristic resistance intersects the descending portion of the load–slip curve, the characteristic slip capacity (δuk) is specifically defined as 0.9 times the minimum test value of δu . Eurocode 4 states that a connector is considered ductile if its characteristic slip capacity (δuk) is at least 6 mm. This criterion indicates a fully plastic shear connection by allowing designers to assume equal loading of all studs at the final limit state [19].

In the absence of shear connectors, the natural bond between steel and concrete exhibits a brittle failure mode. Introducing studs to the flange enhances ductility, meeting Eurocode 4 criteria with a characteristic slip capacity (δuk) just exceeding 6 mm. However, when studs are added to the web, although the ultimate load increases by 40%, δuk falls below 6 mm, no longer meeting Eurocode 4 ductility criteria but maintaining superior ductility compared to a natural bond.

3.3 Mode of failure

The natural bond slip specimen exhibited fewer cracks than those with shear studs. Among the three specimens with increased confinement, embedded length, and cover, most displayed minimal to no cracking compared to the control specimen. Notably, the control specimen (HM00) experienced a distinct failure mode; during the initial loading stage, there was no observable change on the surface of each specimen, whether subjected to monotonic or repeated loads. As the specimen reached 80% of its ultimate capacity, initial cracks became visible, primarily concentrated near the center on the flange side. These cracks quickly propagated with increasing load, extending downward. Those in the middle became more pronounced and expanded in both directions. At approximately 90% of the ultimate load, all cracks became visible. No cracks were observed on either side of the specimen's web face (Figure 3).

Figure 3 reveals that specimens equipped with stud connectors attached to the flange, denoted as HMS1 and HRS1, exhibited notable areas of cracking in contrast to the control specimen HM00. The occurrence of two parallel longitudinal cracks on the flange face was particularly prominent at an 85% load level for both HMS1 and HRS1. These longitudinal cracks originated at the base of the specimen and extended towards its center.

In the case of specimens HMS1 and HMS2, horizontal cracks bridged the two longitudinal cracks, which were situated between the two studs. This bridging effect occurred at load levels of +307 and 430 kN, respectively, following the attainment of ultimate loads at 334 and 472 kN. Subsequently, as the load decreased, diagonal cracks began to emerge, mirroring the behavior observed in repeated load specimens HRS1 and HRS2.

As the slip reached approximately 6 mm, distinct descending steps sequentially appeared, often accompanied by audible sounds. This showed that all of the studs in the steel part had sheared off as shown in Figure 4. The applied load stabilized at the residual load level at a slip of about 9 mm.

3.4 Analyzing the influence of various parameters

Proportional analyses of load–slip responses underscore the crucial role of three key parameters: embedded length, confinement, and encasement cover, especially in shaping the interfacial bond-slip behavior observed in specimens under monotonic and repeated loading conditions. Figure 5

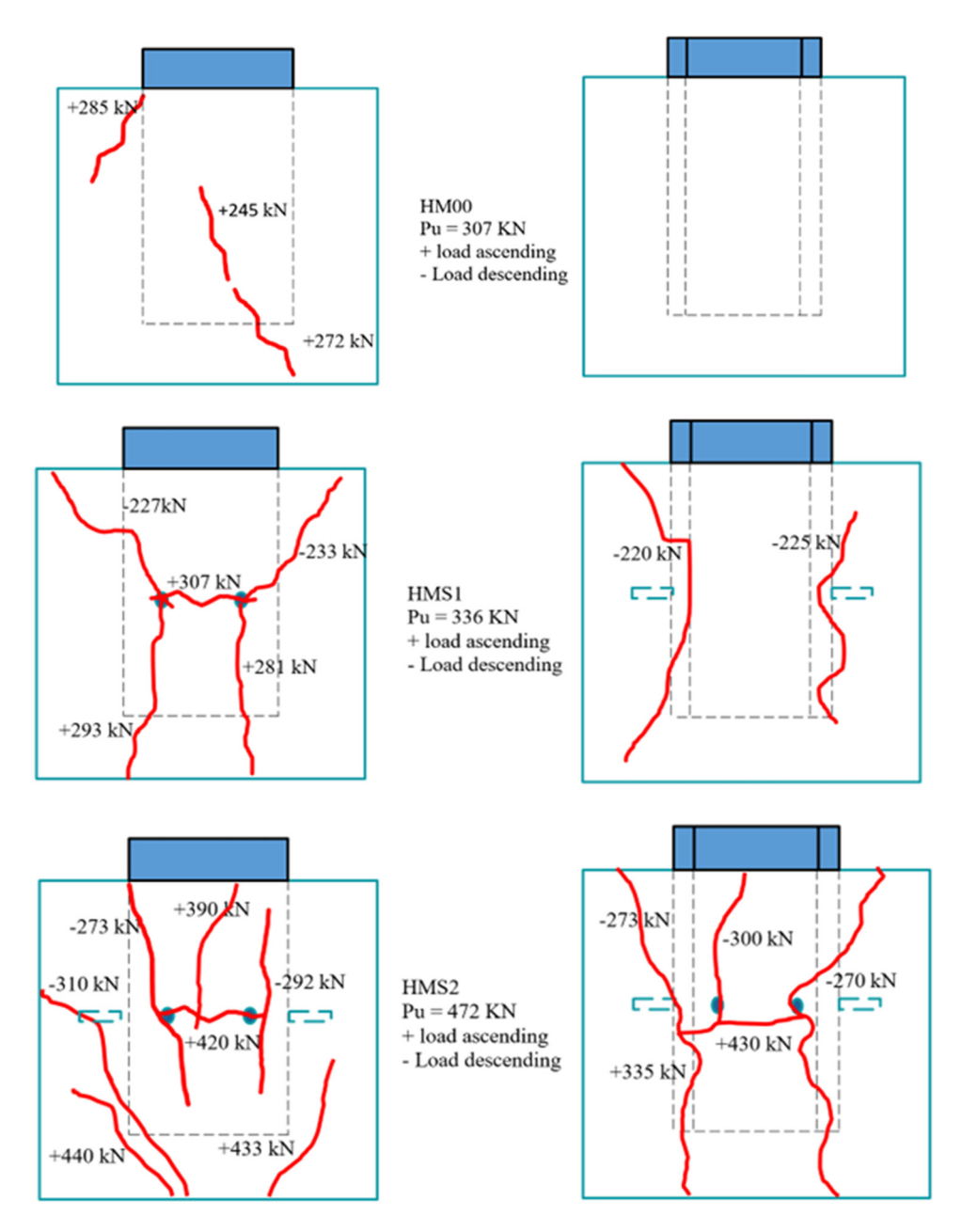


Figure 3: Crack patterns after push-out test.

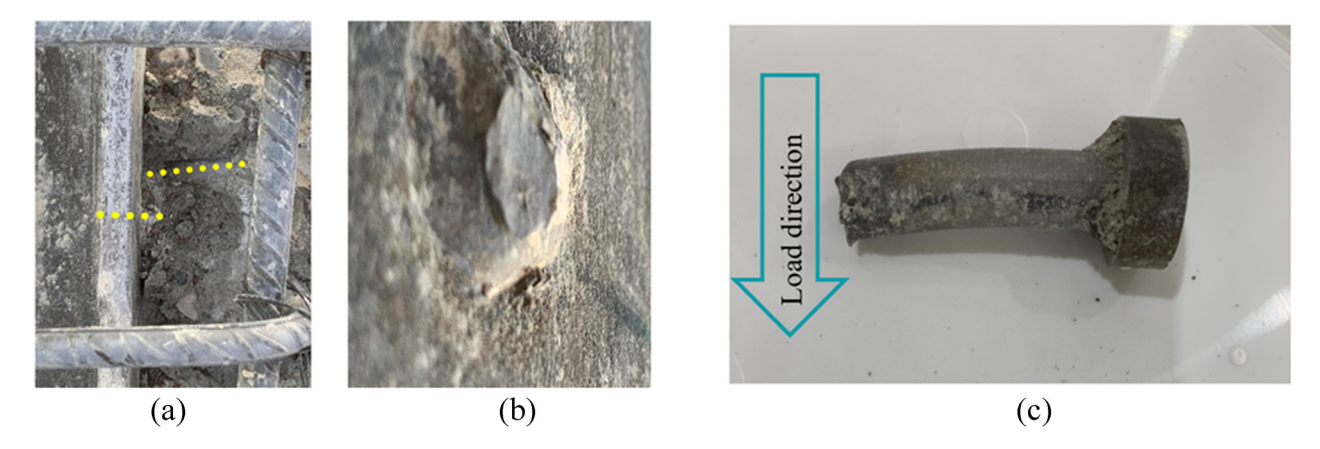


Figure 4: Shear stud failure (a) after encasement remove (b) flange side (c) combine flexural and shear.

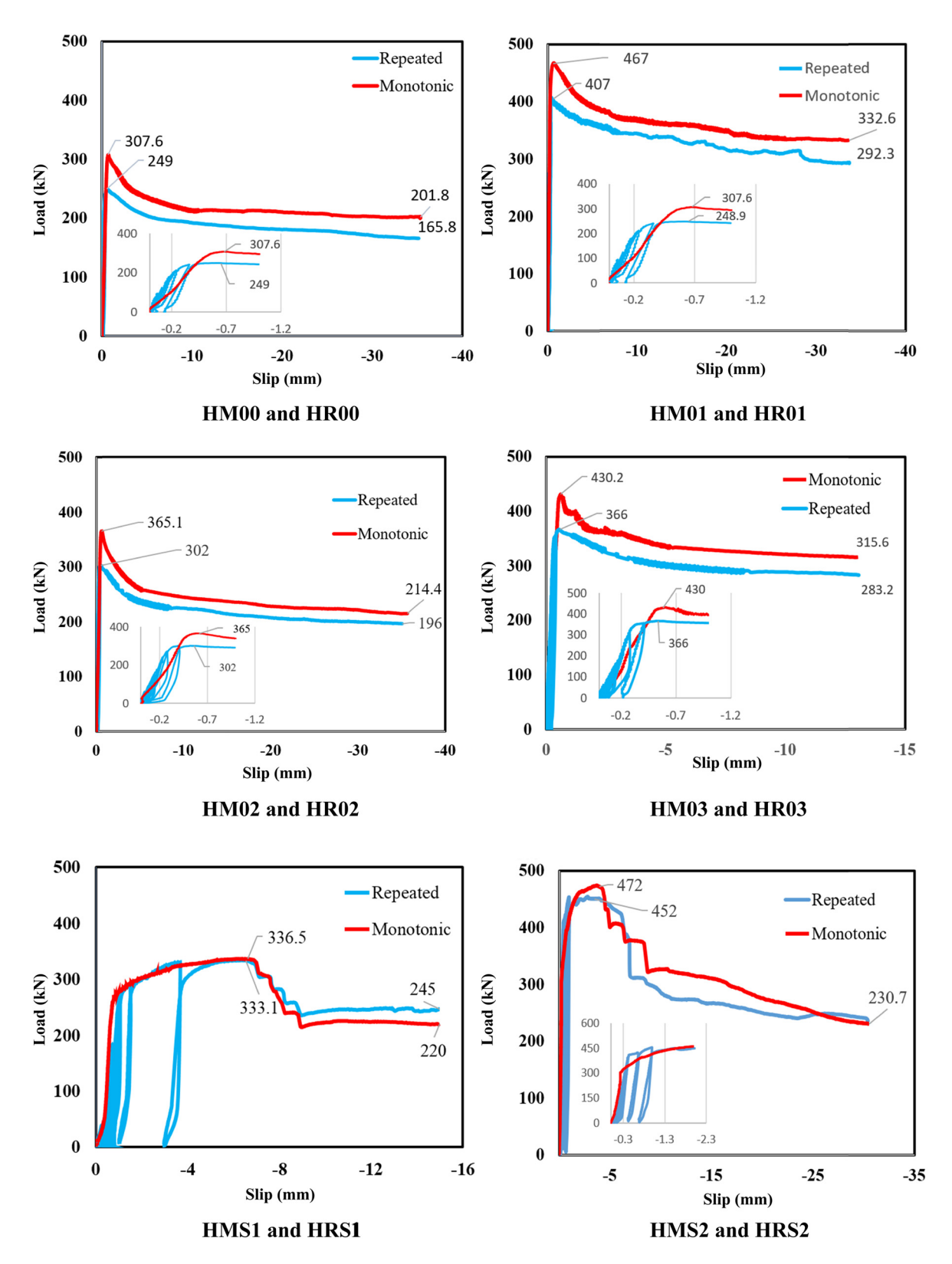


Figure 5: Load-slip curves monotonic and repeated load for all push-out specimens.

sheds light on the influence of loading type on natural bond capacities in specimens (HM00, HM01, HM02, and HM03), revealing lower values for the ultimate load and residual load by (13-18%) and a reduction (8-18%), respectively, with repeated loading. This reduction is attributed to the cumulative effect of repeated loading cycles, inducing micro-cracks within the material and resulting in a diminished load-carrying capacity. Conversely, the higher ultimate load observed in monotonic loading conditions suggests that the specimen can withstand a single, continuous load application more effectively. Furthermore, specimens with shear stud connections (HMS1 and HMS2) experienced a diminished reduction of (0-4%), credited to the enhanced ductility in the load-slip curve. The influence of these parameters is undeniable, significantly impacting ultimate and residual load-bearing capacities.

3.4.1 Embedded length

The comparative assessment of specimens HM01 and HR01 in relation to control specimens HM00 and HR00 involved an increase in the embedded length from 300 to 500 mm while maintaining constant concrete strength and confinement. This translated to a 67% increase in embedded length, significantly improving the load-slip relationship, as shown in Figure 5. In the monotonic load test for HM01, the ultimate load experienced a 50% increase at approximately 0.7 mm slip, and this increment remained constant until the residual load reached 10 mm slip, with the increments in the residual load persisting at 65% at 35-mm slip. For the repeated load specimen HR01, the ultimate load demonstrated a 63% increase, and the residual load showed a 75% increase at 10-mm slip. Interestingly, this increment remained consistent as the slip reached 35 mm in the repeated load test. The observed improvement in repeated load resistance surpassed that in monotonic load, indicating that a greater embedded depth enhances resistance to repeated loading.

3.4.2 Confinement

A comparative evaluation of Specimens HM02 and HR02 about Control Specimens HM00 and HR00 is carried out. The stirrup diameter increased from 10 mm to 12 mm, maintaining an 80 mm spacing; this means raising the stirrup volume ratio from 0.76 to 1%. This led to a significant improvement in the load–slip relationship. In the monotonic load test for HM02, as shown in Figure 5, the ultimate load increased by 19% at approximately 0.6-mm slip, and the residual load increased by 15% at 10 mm,

persisting to 7% at 35 mm. In the repeated load specimen HR02, the ultimate load increased by 21%, and the residual load increased by 15% at 10-mm slip. This increase continued, reaching 18% when the slip reached 35 mm in the repeated load test. The potential for customized reinforcement strategies and raising the stirrup ratio elevated the bond–slip performance under diverse loading conditions. push-out specimens.

3.4.3 Concrete cover

An examination of Specimens HM03 and HR03 in comparison to the control counterparts HM00 and HR00 reveals the impact of doubling the concrete cover from 100 mm to 200 mm in both directions. This alteration significantly improves the load–slip relationship, as shown in Figure 5. In the case of HM03, the ultimate load experiences a 40% increase at around 0.65-mm slip. In comparison, the residual load shows a remarkable surge of 52% at 10-mm slip during the monotonic load test. Likewise, the repeated load test for HR02 demonstrates a 47% increase in the ultimate load and a concurrent 50% rise in the residual load at 10-mm slip.

3.4.4 Shear stud

Conducting a comparative assessment of specimens HMS1 and HRS1 against control specimens HM00 and HR00, the incorporation of shear studs attached to the flange, with two studs on each side, resulted in a noteworthy enhancement in the ductility of the load–slip relationship. In the monotonic load test for HMS1, the ultimate load witnessed a 9% increase at approximately ten times the slip; specifically, the ultimate load reached 336 kN at a 6-mm slip. Subsequently, the load gradually decreased until the residual load stabilized. Notably, the residual load, when compared with the natural bond HM00, remained at the same value. At a slip of 25 mm, as shown in Figure 5. The residual load held steady, revealing a 13% increase compared to the residual load of the deteriorated natural bond specimen.

In the repeated load specimen HRS1, a significant 33% increase in the ultimate load was observed, maintaining consistency with the ultimate load in both monotonic and repeated loads. This suggests that the repeated load exhibited no distinct effect compared to the behavior demonstrated in the HMS1 specimen, which is attributable to its ductility behavior. Additionally, the residual load showed a 26% increase at the same slip of 10 mm.

The concise analysis of specimens HMS2 and HRS2 against control specimens HM00 and HR00 underscores

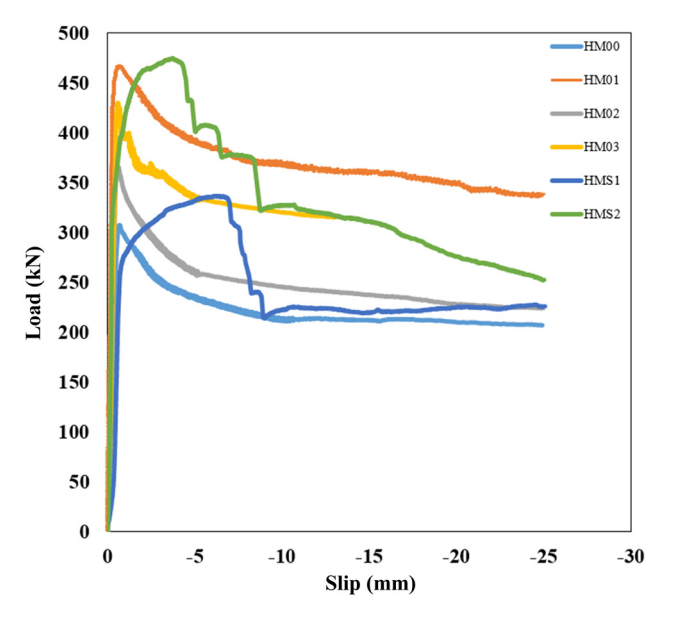


Figure 6: Load-slip curve for all monotonic push-out specimens.

also had significant improvement in load—slip ductility with the integration of shear studs on both flange and web sides; in the monotonic load test for HMS2, the ultimate load increased by 53% at around six times the slip, reaching 472 kN at a 4-mm slip. The residual load, compared to the natural bond HM00, rose by 54% at 10-mm slip, gradually diminishing to zero at 30 mm.

In the repeated load specimen HRS2, a remarkable 83% increase in the ultimate load was observed, accompanied by a substantial 50% increase in the residual load at the same 10-mm slip, highlighting the durability and resilience of the shear-stud-enhanced configuration.

3.5 Summary

In Figure 6, the highest ultimate load value is exhibited by specimen HMS2, where studs are added to both the web and flange. This surpasses the load values of other specimens, including HM01 with an increased embedded length of 67%, HM03 with an increased concrete cover of 100%, and HM02 with an increased confining stirrups ratio of approximately 40%. Particularly, the ultimate load of HMS2 exceeds that of HMS1, where studs are attached to flanges only. However, under repeated loading, the addition of studs demonstrates a remarkable consistency in ultimate load, contrasting with lower (13–18)% ultimate loads and (8–18)% residual loads compared to monotonic loading in other specimens with natural bonds. Furthermore, the presence of studs significantly enhances ductility.

3.6 Strain distribution under varied loads

Theoretical analysis indicates that the strain in H-section steel is zero at x = 0, reaching its peak at 50 mm from the loaded end, signifying maximum bond stress concentration near the loading end. As we move along the embedded length, this bond stress gradually diminishes, reaching its minimum at the free end. Under peak load conditions, the strain decreases to approximately 70% at 50 mm from the free end. Overall, the strain increases across the embedded length with the rising load, as depicted in Figure 7. This progression is more pronounced at the loading end compared to the free end. As the load intensifies, the strain differences between the loading and free ends of the H-

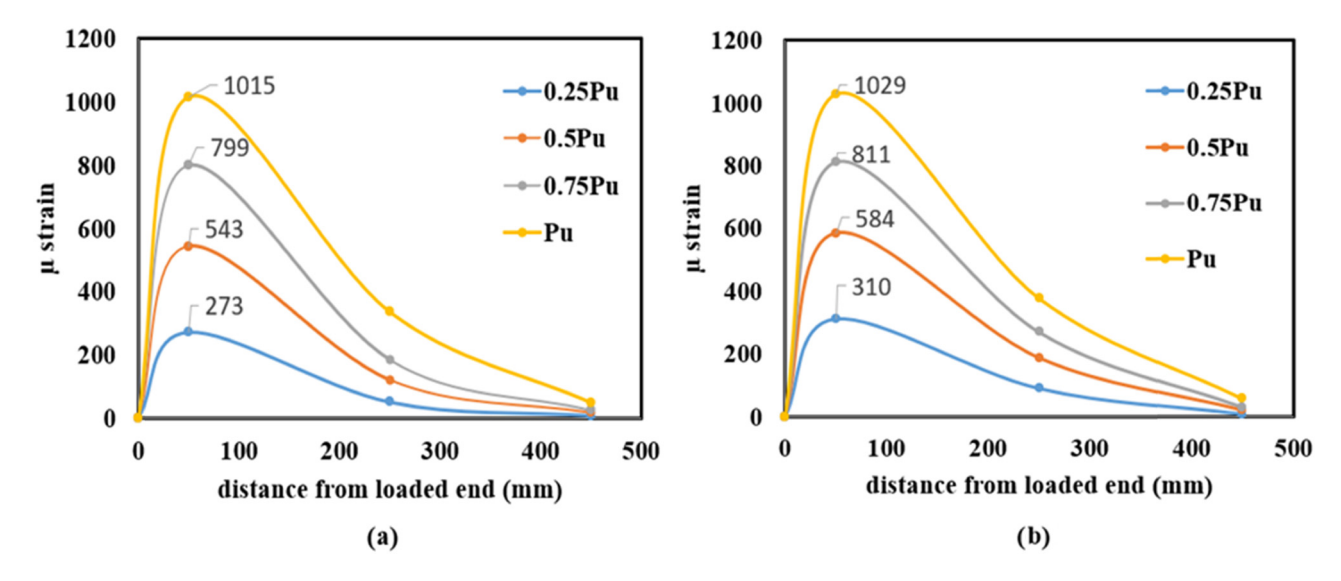


Figure 7: Strain distribution along the embedded depth. (a) Web strain and (b) flange strain.

shaped steel section become more evident, indicating a disruption in the steady transfer of strain at the interface between the H-shaped steel section and the concrete, resulting in relative slip. Additionally, it is worth noting that the strain in the flange exceeds that in the web by a marginal difference not exceeding 6%, suggesting approximate equality.

4 Conclusion

In light of the analysis conducted, several key conclusions emerge from this investigation regarding alternative strategies for enhancing the interaction between H steel sections and concrete.

- The study found that adding 10-mm-diameter studs to both flanges and the web of the steel section is more effective than increasing the embedded depth by 67%.
 The second most effective method is doubling the concrete cover, followed by increasing the stirrups ratio by 40%.
- The addition of studs solely to flanges exceeded only the effect of increasing the stirrup ratio under repeated loading but remained below other enhancement parameters.
- The results demonstrated a notable shift in the load-slip behavior from brittle to ductile when shear studs were employed.
- The additional studs on the web in comparison to studs on flanges only result in an increased ultimate load but a reduced ductility, underscoring the importance of carefully balancing structural strength and deformability.
- The influence of loading type (repeated or monotonic) was markedly evident in the natural bond, with repeated loading consistently resulting in lower (13–18)% ultimate loads and (8–18)% residual loads compared to monotonic loading. However, shear stud connections emerged as a mitigating factor, demonstrating comparable values, mainly when studs were exclusively applied to the flange. The impact persisted when both the flange and web were equipped with studs, albeit with somewhat reduced efficiency.
- The investigation reveals a consistent pattern where the maximum bond stress is concentrated near the loading end, gradually diminishing along the embedded length of the H-section until it reaches its minimum at the free end. Moreover, there is a proportional increase in bond stress with the augmentation of the push-out load.
- The load-slip model was established for natural bond specimens, but limitations in tested specimens and high non-linearity in mechanical stud connections prevented establishing a load-slip model for the latter. Further investigation is

- necessary, particularly exploring different stud dimensions and mechanical connection configurations.
- The strain demonstrates a higher rate of increase with the escalation of load; the strain in the flange exceeds that in the web by a marginal difference not exceeding 6%, suggesting approximate equality.

Acknowledgements: The authors express sincere gratitude for the invaluable support extended by the Laboratory for Structural Materials Testing at Mosul University throughout this study.

Funding information: The authors state no funding involved.

Author contributions: All authors have accepted responsibility for the entire content of this manuscript and consented to its submission to the journal, reviewed all the results, and approved the final version of the manuscript. AAA-J: investigation, resources, data curation, writing original draft, and visualization. SYA-D: conceptualization, methodology, validation, and supervision.

Conflict of interest: Authors state no conflict of interest.

Data availability statement: The authors confirm that the data supporting the findings of this study are available within the article [and/or] its supplementary materials.

References

- [1] Charles Roeder BW, Chmielowski R, Member A, Brown CB, Member H. Shear connector requirements for embedded steel sections. J Struct Eng. 1999;125(2):142–51.
- [2] Al-Abbas B, Abdul Rasoul Z, Hasan D, Rasheed S. Experimental study on ultimate strength of steel tube column filled with reactive powder concrete. Civ Eng J. 2023;9:1344–55.
- [3] Zheng H, Chen Z, Xu J. Bond behavior of H-shaped steel embedded in recycled aggregate concrete under push-out loads. Int J Steel Struct. 2016;16(2):347–60.
- [4] Liu C, Xing L, Liu H, Quan Z, Fu G, Wu J, et al. Numerical study of bond slip between section steel and recycled aggregate concrete with full replacement ratio. Appl Sci. 2020;10(3):887.
- [5] Bai G, Ma J, Liu B, Chen X. Study on the interfacial bond slip constitutive relation of I-section steel and fully recycled aggregate concrete. Constr Build Mater [Internet]. 2020;238:117688. doi: 10. 1016/j.conbuildmat.2019.117688.
- [6] Wang X, Liu Y, Li Y, Lu Y, Li X. Bond behavior and shear transfer of steel section-concrete interface with studs: Testing and modeling. Constr Build Mater. 2020 Dec;264:120251.
- [7] Hamoda A, Emara M, Mansour W. Behavior of steel I-beam embedded in normal and steel fiber reinforced concrete incorporating demountable bolted connectors. Compos Part B Eng. 2019;174(May):106996. doi: 10.1016/j.compositesb.2019.106996.

- [8] Saikali R. Bond behaviour of steel reinforcing bars embedded in ultra-high-performance steel fiber reinforced concreTE. Toronto, Ontario: York University; 2019.
- [9] Al-Obaidy ZSS, Suhaib Yahya Kasim OAS. Anchorage evaluation of steel rebars post-installed in concrete. MSc thesis. Mosul University; 2022.
- [10] Liu Y, Li J, Jiang L, Xian J, Li H, Zhao Y, et al. Mechanism and design method of load transfer into concrete-filled steel tubular arch ribs through perfobond-rib-shear connectors. Buildings. 2023 Mar;13(3):1.
- [11] He S, Fang Z, Fang Y, Liu M, Liu L, Mosallam AS. Experimental study on perfobond strip connector in steel-concrete joints of hybrid bridges. J Constr Steel Res. 2016 Mar;118:169–79.
- [12] Huang Z, Huang X, Li W, Chen C, Li Y, Lin Z, et al. Bond-slip behaviour of H-shaped steel embedded in UHPFRC. Steel Compos Struct. 2021;38(5):563–82.
- [13] Bai L, Yu J, Zhang M, Zhou T. Experimental study on the bond behavior between H-shaped steel and engineered cementitious composites. Constr Build Mater. 2019 Jan;196:214–32.

- [14] Iraqi Standard Specification I.Q.S. Portland Cement. 2010;(5).
- [15] Iraqi Standard Specification I.Q.S. The Aggregate of Natural Source Used in Concrete. 2010;(45).
- [16] ACI 211.1-91. Standard Practice for Selecting and Proportion for Normal Heavyweight and Mass Concrete. ACI Man Concr Pract Part 1 Mater Gen Prop Concr Detroit, Michigan. 1994. p. 38.
- [17] American Society of Testing and Materials (ASTM). Standard Method of Compressive Strength of Cylindrical Concrete. Specimens ASTM C39/C39M-99 West Conshohocken, PA USA; 1999c.
- [18] American Society of Testing and Materials (ASTM). Standard Method for Splitting Tensile Strength of Cylindrical Concrete Specimens. ASTM C496/C496M-96 West Conshohocken, PA USA; 1999d.
- [19] Eurocode 4: Design of Composite Steel and Concrete Structures, Part 1: General rules and rules for building. Brussels: CEN; 2006.